Article

Torque Generation by Axonemal Outer-Arm Dynein

Shin Yamaguchi,[1] Kei Saito,[1] Miki Sutoh,[1] Takayuki Nishizaka,[2] Yoko Y Toyoshima,[1] and Junichiro Yajima[1,*]

[1]Department of Life Sciences, Graduate School of Arts & Sciences, The University of Tokyo, Tokyo, Japan; and [2]Department of Physics, Gakushuin University, Tokyo, Japan

ABSTRACT   Outer-arm dynein is the main engine providing the motive force in cilia. Using three-dimensional tracking microscopy, we found that contrary to previous reports *Tetrahymena* ciliary three-headed outer-arm dynein ($\alpha\beta\gamma$) as well as proteolytically generated two-headed ($\beta\gamma$) and one-headed (α) subparticles showed clockwise rotation of each sliding microtubule around its longitudinal axis in microtubule corkscrewing assays. By measuring the rotational pitch as a function of ATP concentration, we also found that the microtubule corkscrewing pitch is independent of ATP concentration, except at low ATP concentrations where the pitch generated by both three-headed $\alpha\beta\gamma$ and one-headed α exhibited significantly longer pitch. In contrast, the pitch driven by two-headed $\beta\gamma$ did not display this sensitivity. In the assays on lawns containing mixtures of α and $\beta\gamma$ at various ratios, the corkscrewing pitch increased dramatically in a nonlinear fashion as the ratio of α in the mixture increased. Even small proportions of α-subparticle could significantly increase the corkscrewing pitch of the mixture. Our data show that torque generation does not require the three-headed outer-arm dynein ($\alpha\beta\gamma$) but is an intrinsic property of the subparticles of axonemal dyneins and also suggest that each subparticle may have distinct mechanical properties.

INTRODUCTION

Axonemal dynein molecular motors are engines for the rhythmical beating of eukaryotic cilia and flagella, which is driven by a regulated interaction between outer doublet microtubules and axonemal dyneins (1). Axonemal dyneins are composed of outer-arm and inner-arm dyneins according to their location in the axoneme (2). The outer-arm dynein forms heterodimers or heterotrimers consisting of single species of a multisubunit protein complex containing two or three distinct motor domains of dynein heavy chains (3). The inner-arm dyneins comprise multiple species of multisubunit complexes, consisting of a heterodimeric dynein and multiple monomeric dyneins, each containing distinct motor domains of dynein heavy chains (4,5). Each motor domain exhibits repeated cycles of ATP-sensitive interaction to the outer doublet B-tubule to generate the forces that move cilia and flagella (1). Lack of outer-arm dynein in vivo reduced the frequency of flagellar beating, whereas partial loss of inner-arm dyneins caused a reduction in the amplitude of beating (6–8). Furthermore, motility analyses of *Chlamydomonas* mutants lacking any one of the three motor domains of outer-arm dynein heavy chains showed a reduction of swimming speed and the degree of decrease in speed varied depending on the lacking motor domain (9). These in vivo observations indicated that each axonemal dynein as well as each motor domain in an outer-arm dynein complex contribute to ciliary and flagellar functions in different ways.

In an in vitro microtubule sliding assay, isolated *Chlamydomonas* trimeric outer-arm dyneins ($\alpha\beta\gamma$) and outer-arm dynein mutants lacking one or two (β- or γ-subparticle) of the three motor domains have been shown to drive microtubule sliding at different velocities (10,11). It has also been reported that although the β-subparticle of sea urchin dimeric outer-arm dynein caused microtubule sliding, the α-subparticle did not (α and β heavy chains in sea urchin correspond to γ and β in *Chlamydomonas*) (12–14). The α-subparticle of *Tetrahymena* trimeric outer-arm dynein also had no microtubule sliding activity, but the $\beta\gamma$-subparticle could slide microtubules at velocities similar to those measured for intact trimeric outer-arm dynein (α, β, and γ heavy chains in *Tetrahymena* correspond to γ, β, and α in *Chlamydomonas*) (15,16). These results suggested that each motor domain of outer-arm dynein complex has a distinct role in axonemal dynein function. Thus, characterizing the motile properties of both axonemal dynein complex and its distinct motor domains is necessary for understanding the role of axonemal dyneins in ciliary and flagellar motility. In vitro motor activity of outer-arm dyneins has, thus far, only been quantified by microtubule sliding velocities.

As a unique mechanical property of axonemal dyneins, it has been reported that, in an in vitro microtubule motility assay, inner-arm dyneins purified from *Tetrahymena* generated torque that causes sliding microtubules to rotate around their longitudinal axis (17). The rotational pitch of corkscrewing microtubules driven by each monomeric subspecies of *Chlamydomonas* inner-arm dyneins was variable, ranging from 0.2 to 0.5 μm (5), implying that each motor

domain has a distinct torque component in the dynein force-generating stroke. Therefore, the corkscrewing motion of sliding microtubules provides another index to evaluate the motile properties of axonemal dyneins.

We recently developed a three-dimensional (3D) prismatic optical tracking (termed tPOT) microscope, which yields 3D positional information with nanometer-scale accuracy (18). The tPOT is based on the relative displacement of a pair of split images with a wedge prism located at the back-focal plane of the objective. This method has been applied to a conventional in vitro microtubule sliding assay by tracking streptavidin-coated quantum dots (QDs, diameter of ~20 nm) that were bound to a sparsely biotinylated-microtubule sliding across lawns of truncated monomeric kinesin molecules and revealed the corkscrewing motion of microtubules induced by kinesins at saturated ATP concentration (18).

In this study, we applied this tracking method to quantify the microtubule sliding and rotation driven by *Tetrahymena* outer-arm dynein and its subparticles (α and $\beta\gamma$) digested by chymotrypsin (19,20), to examine the motile properties of the outer-arm dynein and its motor domains. We found that *Tetrahymena* ciliary outer-arm three-headed dynein as well as its proteolytically generated subparticles rotated sliding microtubules around their longitudinal axis. We then measured the microtubule corkscrewing motion at various ATP concentrations. Our results suggest that each subparticle may have distinct mechanical properties leading to different motile activities.

MATERIALS AND METHODS

Preparation of outer-arm dynein

Tetrahymena thermophila (strain B-255) were grown in medium containing 1% (w/v) proteose peptone, 0.5% (w/v) yeast extract, 0.87% (w/v) glucose, and a small amount of antifoaming agent (FS Antifoam DB-110N, Dow Corning Toray, Tokyo, Japan) with aeration at 37°C. After collecting cells by low-speed centrifugation, cilia were isolated using the Ca^{2+} shock method (21), and then demembranated with Nonidet-P40. The isolated axonemes were resuspended in 0.6 M NaCl, 10 mM HEPES, pH 7.4, 4 mM $MgCl_2$, 0.1 mM EGTA, and 1 mM phenylmethylsulfonyl fluoride (PMSF), left to stand for 30 min at 0°C, and centrifuged at $40,000 \times g$ for 10 min. The supernatant was fractionated on a 30 ml with 5–20% (w/w) sucrose density gradient in a solution of 0.1 M NaCl, 4 mM $MgCl_2$, 0.1 mM EGTA, 1 mM dithiothreitol (DTT), 0.1 mM ATP (Grade II, Sigma-Aldrich, St. Louis, MO), 0.1 mM PMSF and 10 mM HEPES, pH 7.4. After sedimentation at $89,000 \times g$ for 16 h at 4°C in a P28S ultracentrifuge rotor (CP70MX, Hitachi Koki, Tokyo, Japan), the gradient was separated into 20–22 fractions and the fractions containing the dynein protein peak were pooled (P1: $\alpha\beta\gamma$).

Proteolytic digestion of outer-arm dynein by chymotrypsin

Outer-arm dynein (P1: $\alpha\beta\gamma$) was digested into one-headed α- and two-headed $\beta\gamma$-subparticles by chymotrypsin (Sigma-Aldrich). Digestion was started by adding chymotrypsin to 0.02 mg ml^{-1} at 25°C, and terminated by adding PMSF to 1 mM. Grades of digestion are classified into three stages (20). Extended digestion results in the loss of motility (data not

shown), so the digestion time was carefully optimized. For purification of the α-subparticles, digestion was terminated before band 4 appeared (see Fig. S1 in the Supporting Material, there is no band at number 4) (20). For purification of the $\beta\gamma$-subparticle, because the $\beta\gamma$-subparticle and intact outer-arm dynein could not be resolved adequately by a Mono Q 5/50 GL ion-exchange column (GE Healthcare, Buckinhamshire, UK), digestion was continued until band 1 (α-subparticle) had disappeared, indicating that no intact outer-arm dynein remains (20).

Purification of outer-arm dynein ($\alpha\beta\gamma$) and subparticles (α or $\beta\gamma$) by Mono Q column

The pooled fraction (P1: $\alpha\beta\gamma$) or digests containing α- or $\beta\gamma$-subparticles were purified further by binding to a Mono Q 5/50 GL ion-exchange column equilibrated with H-buffer (4 mM $MgCl_2$, 0.1 mM EGTA, 1 mM DTT, 0.1 mM PMSF, 0.1 mM ATP, and 10 mM HEPES, pH 7.4, 10% (w/v) sucrose), and then eluting with 20 ml of a 0.05–0.6 M NaCl gradient in the same buffer at a flow rate of 0.5 ml min^{-1}. $\alpha\beta\gamma$, α-subparticles, and $\beta\gamma$-subparticles were eluted at 300–350 mM, 170–200 mM, and 280–330 mM NaCl, respectively. The peak fractions were pooled and then concentrated and exchanged into H-buffer using centrifugal filters (Amicon Ultra-0.5, Ultracel-100 membrane, Merck Millipore, Billerica, MA). Purified $\alpha\beta\gamma$, α, and $\beta\gamma$ were flash frozen and stored in liquid N_2. Dynein concentrations were estimated by sodium dodecyl sulfate polyacrylamide gel electrophoresis (SDS-PAGE) on 7.5% acrylamide gels using bovine serum albumin (BSA) standards (Thermo Fisher Scientific, Waltham, MA) loaded on the same gel. Gels were stained with Quick-CBB PLUS (Wako Pure Chemical Industries, Osaka, Japan) and imaged using a CCD camera (CSFX36BC3, Toshiba Teli, Tokyo, Japan). The bands containing dyneins and BSA standards were quantified using Quantity One software (Bio-Rad, Hercules, CA).

Preparation of QD-coated microtubules

For motility assays, sparsely biotinylated, rhodamine-labeled paclitaxel-stabilized microtubules were prepared. Tubulin was purified from porcine brain by cycles of polymerization and depolymerization followed by phosphocellulose chromatography as previously described (22). Biotinylated (Biotin-(AC5)2-Sulfo-OSu, Dojindo, Kumamoto, Japan), rhodamine-labeled (5-(and-6)-Carboxy-X-rhodamine, Invitrogen, Carlsbad, CA) microtubules were prepared by copolymerizing biotinylated, rhodamine-labeled, and nonfluorescent tubulin in a molar ratio of 1:5:170 in BRB80 (80 mM PIPES, pH 6.8, 1 mM $MgCl_2$, 1 mM EGTA) with 1 mM $MgCl_2$ and 1 mM GTP for 30 min at 37°C and then stabilized by addition of 40 μM paclitaxel (Sigma-Aldrich) (18). QD-coated microtubules were prepared by adding 10 nM streptavidin-coated QD (Invitrogen) diluted in BRB80 containing 20 μM paclitaxel (BRB80T), and incubated for 20–60 min with an equal volume of 0.1 mg ml^{-1} microtubules and then diluted to 0.6 nM QD and 6 μg ml^{-1} microtubules in BRB80T containing 0.4 mg ml^{-1} casein (Nacalai Tesque, Kyoto, Japan). To prepare guanosine-5′-[(α,β)-methyleno]triphosphate (GMP-CPP) microtubules, the mixture of biotinylated, rhodamine-labeled, and nonfluorescent tubulin were exchanged into BRB80 containing 20 μM GMP-CPP (Jena Bioscience, Jena, Germany) twice using centrifugal filters (Amicon Ultra-0.5, Ultracel-30 membrane, Millipore). The mixture was then copolymerized with 0.4 mM GMP-CPP for 60 min at 37°C. QD-coated GMP-CPP microtubules were prepared as described except that BRB80 was used instead of BRB80T.

Microtubule sliding and rotation in 3D motility assays

Microtubule motility assays were performed in flow chambers assembled from two coverslips attached together using double-sided tape (NW-25, Nichiban, Tokyo, Japan). $\alpha\beta\gamma$, $\beta\gamma$, or α were diluted with H-buffer containing

0.5 M NaCl to a concentration of 0.25 M NaCl and incubated on ice. Each dynein was then diluted to 0.1 μM ($\alpha\beta\gamma$), 0.8 μM ($\beta\gamma$), and 1.5 μM (α) with H-buffer containing 0.25 M NaCl immediately before the assay. To assay the mixture of α- and $\beta\gamma$-subparticles, solutions containing 0.8 μM of $\beta\gamma$ and 0.8 μM of α-subparticles were mixed at various ratios 1 min before the assay, giving final concentrations of 0.1 and 0.7 μM, 0.3 and 0.5 μM, 0.4 and 0.4 μM of α and $\beta\gamma$, respectively. 1 volume of the dynein solution was introduced into the flow chamber and incubated for 3 min. The chamber surface was then coated with 4 volumes of 1 mg ml^{-1} casein (Nacalai) in 50 K-Ace buffer (10 mM PIPES, 50 mM potassium acetate, 4 mM MgSO$_4$, 1 mM EGTA, pH 7.4) for 2 min, and then rinsed with 4 volumes of 50 K-Ace buffer. 2 volumes of sparsely biotinylated, rhodamine-labeled microtubules bound to streptavidin-coated QDs in BRB80 containing 20 μM paclitaxel and 0.4 mg ml^{-1} casein were then added and incubated for 2 min, and then rinsed with 2 volumes of 50 K-Ace buffer. Finally, 2 volumes of 50 K-Ace buffer containing 1–100 μM ATP (BioXtra, Sigma-Aldrich), ATP regeneration, and oxygen scavenger systems (23), 1 mM DTT and 20 μM paclitaxel were applied to the chamber. For assays using GMP-CPP microtubules, paclitaxel was not added to the solution. The chamber was sealed with nail varnish. Assays were carried out at room temperature (24 $\pm$ 1°C).

3D tracking microscopy

The 3D tracking microscope was constructed as described previously (18). As a schematic illustration of the tPOT setup is in Fig. 1 A, the back-focal-plane (BFP) of the objective was focused outside the camera port of an inverted microscope (the dotted-line box, TE2000-U, Nikon, Tokyo, Japan) with achromatic lens-1 (combined focal length 50 mm) to make an equivalent BFP (eBFP). A custom-made wedge prism (86.5°) coated with an antireflective layer was precisely located at the eBFP. The two split images of a sample were focused on the camera focal plane by achromatic lens-2 (combined focal length 120 mm), which determined the magnification of the optical system. Images were recorded by EMCCD camera (iXon X$_3$ DU897, Andor Technology, Belfast, UK) at 1.0 to 2.0 s intervals for assays at 1 μM ATP, 0.5 s at 3 μM ATP, 0.1 to 0.2 s at 10 μM ATP, 0.05 to 0.1 s at 30 μM ATP, and 0.03 to 0.1 s at 100 μM ATP. Rhodamine-labeled microtubules and QDs were illuminated using a mercury lump (Intensilight, Nikon). For calibration of the z-axis position the objective was displaced at a constant speed using a custom-built stable stage (ChuukoushaSeisakujo, Tokyo, Japan) equipped with a pulse motor (SGSP-13ACT, Sigma Koki, Tokyo, Japan) and controller (QT-CM2, Chuo Precision Industrial, Tokyo, Japan).

RESULTS AND DISCUSSION

Outer-arm dyneins slide microtubules with a corkscrew motion

We have developed a 3D prismatic optical tracking (tPOT) system based on the relative displacement of a pair of spilt images divided by a wedge prism to quantify microtubule corkscrewing motion driven by kinesins (18). The tPOT system was used to examine if outer-arm dyneins also drive microtubules with a corkscrewing motion in an in vitro motility assay (Fig. 1).

Three-headed outer-arm dyneins ($\alpha\beta\gamma$) were extracted from *Tetrahymena* axonemes using high-salt buffer, and then purified by velocity sedimentation on sucrose density gradients followed by ion-exchange chromatography (see Materials and Methods and Fig. S1). To quantify the motion of the moving microtubules driven by outer-arm dyneins,

we determined the *xyz* position of streptavidin-coated QDs (diameter of ~20 nm) that were bound to sparsely biotinylated microtubules sliding across a surface coated with outer-arm dyneins (Fig. 1 B). The z-directed displacement of the QDs bound to the moving microtubules was provided by the difference between the two image positions of QDs in the y-direction at an equivalent sample plane (the camera plate), whereas the x and y positions of the QDs were obtained from the average of the two image positions (Fig. 1 C, see also Movie S1). Plots of the x-y trajectory (Fig. 1 D red, where x is parallel and y is perpendicular to the direction of microtubule sliding with both parallel to the glass surface) and x-z trajectory (Fig. 1 D blue, perpendicular to the glass surface) of a QD bound to a microtubule in the presence of 10 μM ATP showed oscillations, indicating that sliding microtubules rotate around their longitudinal axis. For the microtubule in Fig. 1 D, fitting the x-y trajectory of the QD position with a sine function gave a rotational pitch of 0.81 μm. The corresponding y-z trajectory was circular (Fig. 1 E) and θ varied linearly as time increased in the range $-180° < \theta < 180°$ (Fig. 1 F), allowing determination of the handedness of the corkscrewing motion of the microtubule. The microtubule rotated in a clockwise direction as viewed from the microtubule minus end (i.e., a right-handed corkscrewing motion). The handedness was also checked by the phase lag between the sinusoidal oscillations of the x-y and x-z trajectories (Fig. 1 D) or by 3D plots viewed from the appropriate angle (Fig. 1 G). For the microtubule in Fig. 1 D, the sliding and rotational velocities of the corkscrewing motion were obtained from the slope of the lines of best fit to the x-displacements or revolutions versus time, giving values of 0.21 μm s^{-1} and 0.26 revolutions s^{-1}, respectively (Fig. 1, H and I). This corkscrewing motion demonstrates that $\alpha\beta\gamma$ dynein generates torsional as well as axial sliding forces in microtubule gliding assays.

This right-handed corkscrew (clockwise rotation) is the same handedness as that observed for inner-arm dyneins (5,17,24) and kinesin-14 (25), which move toward the microtubule minus end, whereas plus-end-directed kinesins have opposite handedness with single-headed kinesin-1 (26), kinesin-5 (18) and double-headed kinesin-2 (27), kinesin-5 (18), kinesin-8 (28) driving anticlockwise rotation as viewed from the microtubule plus end. Thus, both axonemal outer- and inner-arm dyneins have the intrinsic property of rotating microtubules clockwise as they slide. However, the outer-arm $\alpha\beta\gamma$ dyneins generated a pitch of 0.76 μm (Table 1), which is larger than the pitch of 0.25–0.54 μm generated by inner-arm dyneins (17,24).

Previous studies did not find any rotation of sliding microtubules driven by outer-arm dyneins from a variety of sources including *Tetrahymena* (11,17). However, these conventional two-dimensional microtubule sliding assays used single microtubules grown from curved axonemal outer doublets several micrometers long as rotational
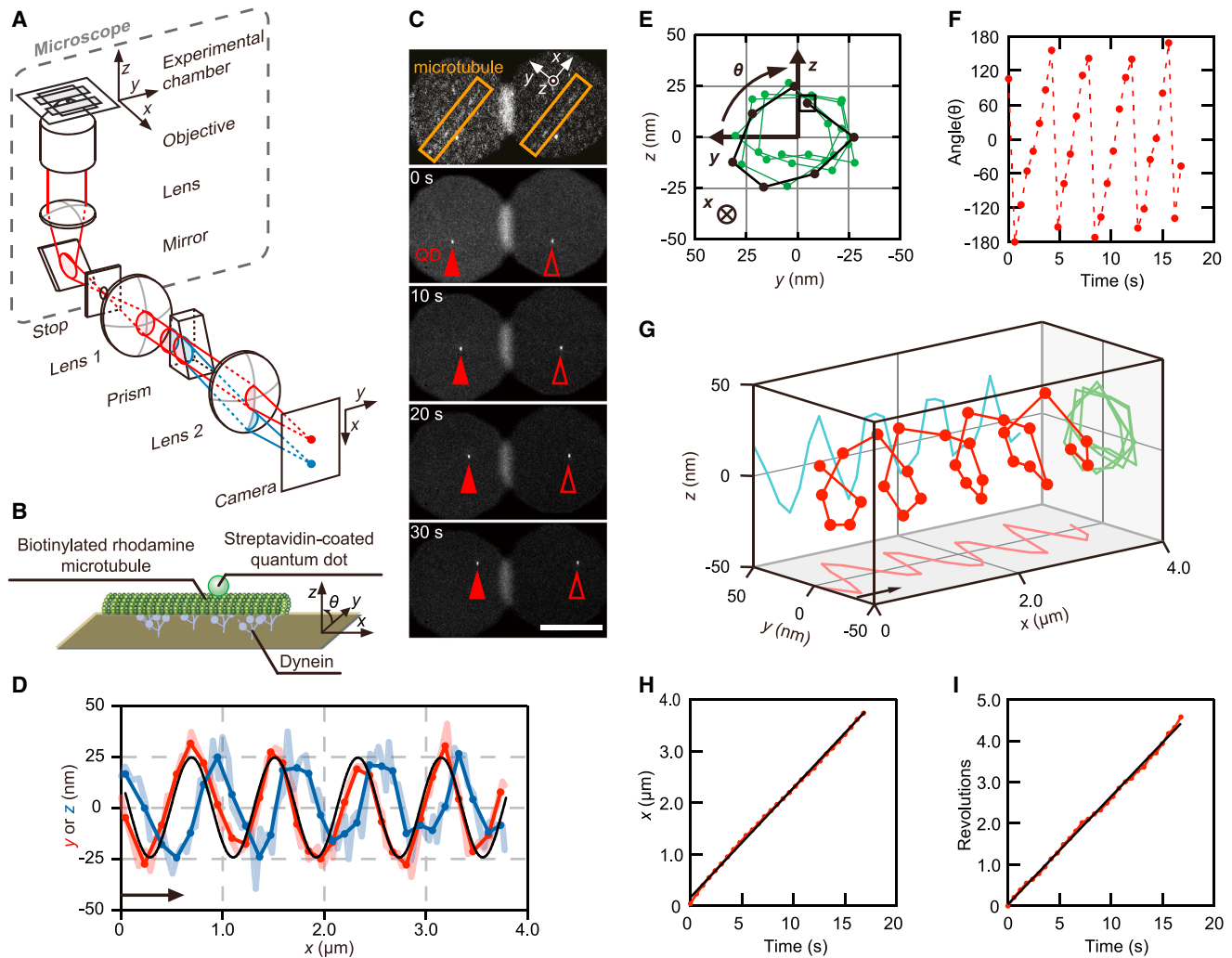
FIGURE 1 Quantification of the corkscrew motion of a sliding microtubule driven by three-headed outer-arm dyneins ($\alpha\beta\gamma$) using 3D tracking microscopy. (*A*) A schematic illustration of the tPOT setup. The beam flux focused by lens-1 outside the camera port of the microscope is split in two by the prism located at an eBFP of the objective. One half-beam of the light passes through the center of lens-2 (*red*), whereas the other half, refracted by the prism, passes below the center (*blue*). Two split beam images were formed on the camera chip with lens-2. (*B*) Diagram of the in vitro microtubule corkscrewing assay during 3D measurement. The sparsely biotinylated, rhodamine-labeled microtubule with a QD ($\lambda = 525$ nm) attached is sliding and rotating driven by *Tetrahymena* dyneins anchored to nonspecifically the glass surface. θ is the rotational angle of the QD around the microtubule's longitudinal axis. (*C*) Sequential images of the microtubule-attached QD observed under the tPOT microscope. The top image shows a rhodamine-labeled microtubule, whereas the others show a QD attached to the translocating microtubule. The solid and open arrowheads indicate the images split by the prism of QD bound to the microtubule, respectively (*time in seconds*). Scale bar, 10 μm. (*D*) The *x-y* (*red*) and *x-z* (*blue*) trajectories of the QD bound to a microtubule shown in (*C*). The rotational pitch was determined by fitting the *x-y* position of the QD with a sine function (*back line*), yielding a value of 0.81 μm. The handedness of the rotation was checked by combining the *x-y* trajectory with the *x-z* trajectory of the QD, because the phase of sinusoidal oscillation of the two traces shifted with a quarter of the wavelength as the sliding microtubules rotated around their longitudinal axis. Images were recorded at 0.2 s intervals (*light red and light blue lines*), and three images were averaged (*red and blue solid lines*). The arrow indicates the approximate displacement during 3 s. (*E*) The *y-z* trajectory of the QD bound to the microtubule shown in (*C*). The trajectory of the first revolution is shown by the black line and begins at the open square. The trajectory shows clockwise rotation of the sliding microtubule when looking in the direction of forward translocation. (*F*) The angle of rotation on the *y-z* plane as shown in (*E*) was plotted against time. The angle (θ) in every rotation increased, indicating a right-handed corkscrew motion in the *xyz* axes defined here. (*G*) 3D plot of the QD shown in (*D*) reveals clockwise rotation of the sliding microtubule. The arrow indicates the approximate displacement during 3 s. (*H*) Time course of *x*-displacement of the QD shown in (*D*). (*I*) Time course of revolution of the QD is shown in (*D*). Revolutions were obtained by shifting the values after each full rotation by 360° shown in (*F*).

markers. We speculate that these projecting axonemes may have hindered rotation in the conventional assays, whereas the 20 nm QD in this assay was sufficiently small to avoid steric hindrance of the sliding microtubules rotation (Fig. 1 *B*, see also Fig. S2).

Microtubule protofilament number does not determine the microtubule corkscrewing pitch driven by dynein

The number of protofilaments in a microtubule assembled in vitro depends on tubulin polymerization conditions.

TABLE 1   Summary of microtubule corkscrew motion

ATP	$\alpha\beta\gamma$			$\beta\gamma$		
Concentration (μM)	Pitch (μm)	Sliding velocity (μm/s)	Rotational velocity (rev/s)	Pitch (μm)	Sliding velocity (μm/s)	Rotational velocity (rev/s)
1	1.6 $\pm$ 0.5 (13/15)	0.020 $\pm$ 0.004	0.014 $\pm$ 0.005	0.81 $\pm$ 0.23 (19/27)	0.035 $\pm$ 0.009	0.049 $\pm$ 0.024
3	0.84 $\pm$ 0.15 (16/16)	0.082 $\pm$ 0.017	0.10 $\pm$ 0.03	0.71 $\pm$ 0.12 (8/11)	0.13 $\pm$ 0.03	0.18 $\pm$ 0.07
10	0.76 $\pm$ 0.17 (96/101)	0.23 $\pm$ 0.06	0.32 $\pm$ 0.13	0.62 $\pm$ 0.10 (27/34)	0.33 $\pm$ 0.08	0.55 $\pm$ 0.16
30	0.75 $\pm$ 0.14 (6/6)	0.66 $\pm$ 0.15	0.90 $\pm$ 0.20	0.67 $\pm$ 0.13 (13/13)	0.93 $\pm$ 0.10	1.4 $\pm$ 0.3
100	0.61 $\pm$ 0.12 (5/5)	1.7 $\pm$ 0.5	2.9 $\pm$ 1.1	0.86 $\pm$ 0.16 (8/14)	2.4 $\pm$ 0.4	2.8 $\pm$ 0.3
	α					
1	2.1 $\pm$ 0.3 (9/12)	0.010 $\pm$ 0.002	0.005 $\pm$ 0.001			
3	0.66 $\pm$ 0.09 (15/15)	0.076 $\pm$ 0.016	0.12 $\pm$ 0.03			
10	0.45 $\pm$ 0.07 (15/15)	0.32 $\pm$ 0.06	0.75 $\pm$ 0.18			
30	0.43 $\pm$ 0.05 (19/19)	0.84 $\pm$ 0.16	2.0 $\pm$ 0.4			
100	0.42 $\pm$ 0.05 (12/13)	1.8 $\pm$ 0.3	4.4 $\pm$ 0.9			

In assays using either $\alpha\beta\gamma$, $\beta\gamma$, or α dynein, of 143, 99, and 74 sliding QD-attached microtubules, 136, 75, and 70 rotated. The other 7, 24, and 4 did not rotate. All rotated clockwise as viewed from the microtubule minus end. Only microtubules >2 μm length were analyzed and only microtubules that clearly rotated >1.5 revolutions were scored as rotating. Values of denominator in parentheses are the number of microtubules analyzed and values of the numerator are the number of microtubules rotated. Errors are standard deviations.

In 13-protofilament microtubules, the protofilaments are paraxial to the microtubule longitudinal axis, whereas in 14-protofilament microtubules they have a left-handed twisted-protofilament lattice of ~ –6 μm (the minus sign refers to a left-handed helical path over the microtubule surface). Our previous work found that tubulin polymerization in the presence of 1 mM GTP in BRB80 forms a 5:3 mixture of 13- and 14-protofilament microtubules (18). Using microtubules in this mixture, we examined microtubule corkscrewing motion driven by three-headed $\alpha\beta\gamma$ dyneins in the presence of 10 μM ATP. We observed the movement of 272 QDs on different microtubules. We rejected 171 of the QD traces because the QD signal was too weak to quantify or a perturbing event such as microtubule crossing occurred. In the remaining 101 events, the $\alpha\beta\gamma$ dynein rotated 96 microtubules clockwise. We plotted the frequency distribution of corkscrewing pitch in a histogram and fitted this with a Gaussian function, giving a mean pitch of +0.73 $\pm$ 0.18 μm (mean $\pm$ SD, n = 96) (Fig. S3). The other five microtubules showed sliding but no rotation (see Table 1 for other conditions). We also examined corkscrewing of microtubules assembled in the presence of GMP-CPP, where >95% of the microtubules have 14-protofilaments (29,30). We analyzed 60 of the QD traces. In 55 events, the $\alpha\beta\gamma$ dynein rotated sliding microtubules. These microtubules also had a right-handed rotation with a pitch of +0.72 $\pm$ 0.18 μm (mean $\pm$ SD, n = 55) (Fig. S3). In the other five events, $\alpha\beta\gamma$ did not rotate GMP-CPP stabilized microtubules. There was no significant difference in the corkscrewing pitch of microtubules assembled with either GTP or GMP-CPP (p = 0.52 in t-test). The microtubule corkscrewing pitch at ~0.7 μm is shorter than the helical pitch of microtubule protofilaments (31) and larger than those of the three-start monomer helix and the five- and eight-start dimer helices of 13-protofilament microtubules, which are respectively

–12.3, +41, and –65.6 nm (32). We also found that the corkscrewing pitch generated by dyneins was not correlated to microtubule lengths in the range 2–30 μm (Fig. S4). Therefore, we conclude that the outer-arm dynein $\alpha\beta\gamma$-induced microtubule corkscrewing motion is not directly related to either helical tubulin patterns in the microtubule lattice or microtubule length. Microtubule rotation by inner-arm dyneins is also unrelated to microtubule lattice geometry (17).

Proteolytic subparticles of outer-arm dynein also drive microtubule corkscrewing

To determine if all three heads of outer-arm dyneins are needed to drive microtubule corkscrewing, we used our tPOT microscope to track microtubule sliding over surfaces coated with subparticles of *Tetrahymena* outer-arm dynein. Two-headed ($\beta\gamma$) and one-headed (α) subparticles of three-headed outer-arm dyneins ($\alpha\beta\gamma$) were prepared by chymotryptic digestion of three-headed outer-arm dyneins purified by velocity sedimentation on sucrose gradients and ion-exchange chromatography (Fig. S1) (19,20).

We found that both the α-subparticle and $\beta\gamma$-subparticle were able to drive microtubule sliding (Table 1). This contrasts with previous reports where the α-subparticle was found not to slide microtubules in vitro and was therefore proposed to have only a regulatory function (15) (16). At high concentrations of α-subparticles (0.8 μM), α-subparticle driven microtubule sliding was observed using either casein or BSA to block the surface. However, at low concentrations of the α-subparticles (0.1 μM), as used in previous studies (15,16), most microtubules slid smoothly using casein to block the glass surface, but did not slide using BSA instead of casein.

We also found that the $\beta\gamma$ and α dynein proteolytic subparticles drove right-handed corkscrewing of sliding microtubules (Fig. 2, *A* and *B*), with mean rotational pitches
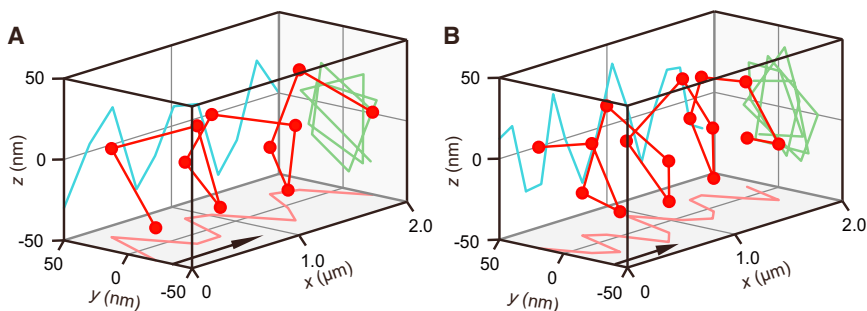
FIGURE 2 Corkscrewing motion of a sliding microtubule driven by outer-arm dynein's proteolytically generated subparticles. 3D plot of the QD bound to a sliding microtubule driven by two-headed $\beta\gamma$ (A) and one-headed α (B) reveals clockwise rotation. The pitch value of each corkscrewing motion is 0.75 μm (A) and 0.52 μm (B). Images were recorded at 0.2 s interval and three images were averaged. Arrows indicate the approximate displacement during 3 s.

of $+0.62 \pm 0.10$ μm (mean $\pm$ SD) and $+0.45 \pm 0.07$ μm (mean $\pm$ SD), respectively, in the presence of 10 μM ATP, which is smaller than the pitch of $+0.76 \pm 0.17$ μm (mean $\pm$ SD) generated by whole $\alpha\beta\gamma$ dyneins ($p <$ 0.001 in t-test) (Table 1). Therefore, torque generation does not require the three-headed outer-arm dynein ($\alpha\beta\gamma$) but is an intrinsic property of one-headed α-subparticles and two-headed $\beta\gamma$-subparticles of axonemal dyneins.

ATP concentration affects dynein-driven microtubule corkscrewing motion

We next asked whether the axial and rotational components of force generated by outer-arm dyneins are coupled in a fixed ratio to the turnover of ATP. In *Tetrahymena* inner-arm dyneins, both components of force were similarly coupled to the turnover of ATP (17). However, the inner-arm dynein subspecies g in *Chlamydomonas* displayed different ATP concentration dependencies for sliding and rotational velocities (5). Because pitch is sliding velocity divided by rotational velocity, the pitch of *Tetrahymena* inner-arm dyneins was constant ($+0.5$ μm) at various ATP concentrations, whereas the pitch of *Chlamydomonas* subspecies g was variable ranging between $+0.2$ and $+0.5$ μm. To determine the relationship between pitch and ATP concentration for *Tetrahymena* outer-arm dyneins, we examined microtubule corkscrewing motion driven by either $\alpha\beta\gamma$, $\beta\gamma$, or α within a range of 1–100 μM ATP. As ATP concentration reduced to 1 μM the pitch increased dramatically to 1.6 μm for $\alpha\beta\gamma$ and 2.1 μm for α, whereas the pitch driven by $\beta\gamma$ was not significantly altered with a mean pitch of 0.74 μm across all ATP concentrations (Fig. 3 A and Table 1, see also Fig. S5), as observed with *Tetrahymena* inner-arm dynein (17). Hence, for both three-headed $\alpha\beta\gamma$ and one-headed α sliding and twisting forces are not coupled in fixed ratios to the turnover of ATP, whereas for two-headed $\beta\gamma$ these forces are coupled to ATP in similar ratios from 1 to 100 μM ATP.

What controls the dynein-driven microtubule corkscrewing pitch at low ATP concentration? There are several potential mechanisms including differences in the mechanical properties, mechanochemistry, or power stroke mechanisms between the subparticles. Because at low concentrations of ATP the dynein heads spend a longer time attached to the

microtubule in a rigor bound state this suggests, as one possible mechanism, that differences in the properties of the rigor bound subparticles in the ATP-waiting state may be significant. Frictional drag caused by the cross-bridge force between dyneins and the microtubule during the ATP-waiting state causes axial and off-axial frictional resistances, limiting the sliding and rotational velocities, respectively. If the α-driven microtubule twisting force is impaired by the off-axial frictional resistance produced by the rigor complex of α, and the α-driven microtubule sliding force is less affected by the relatively small axial frictional resistance, this would result in a longer corkscrewing pitch at low ATP concentrations. Our result shows that the rotational velocity of α indeed decreases faster than sliding velocity as ATP concentration decreases (Fig. 3, B and C, *triangle*), resulting in an increase in pitch (Fig. 3 A, *triangle*). Conversely, $\beta\gamma$, which showed a constant corkscrewing pitch across all ATP concentrations (Fig. 3 A, *square*), would in the ATP-waiting state have identical frictional resistance in both the sliding and rotational directions, affecting equally the sliding and rotational velocities (Fig. 3, B and C, *square*). The different mechanical properties of subparticles may correspond to the distinct dynein subclass of the heavy chains (33), structural differences in the monomer form (α) versus dimer form ($\beta\gamma$), or an alternation in the mechanical properties of the $\beta\gamma$-subparticles during their preparation by proteolysis. Currently, we cannot distinguish between these possibilities.

The effect of combining subparticles with different mechanical properties on microtubule corkscrewing motion

The ATP-concentration dependency of corkscrewing pitch by three-headed $\alpha\beta\gamma$ was similar to that of one-headed α but different from that of two-headed $\beta\gamma$ (Fig. 3 A), implying that the properties of α-subunit in three-headed $\alpha\beta\gamma$ form may contribute greatly to the motile properties of three-headed $\alpha\beta\gamma$. To examine the effect of combining subparticles with different mechanical properties on microtubule corkscrewing motion, we ran tug-of-war microtubule corkscrewing assays where microtubules translocated on mixed surfaces of α and $\beta\gamma$ ($\alpha+\beta\gamma$) subparticles, at constant total motor concentration (Fig. S6). At 1 μM ATP,
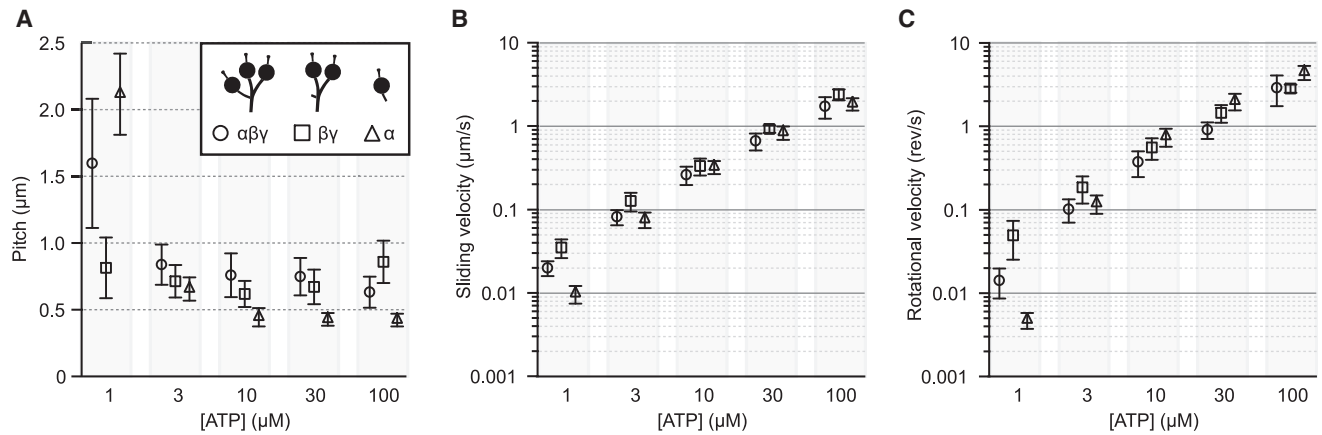
FIGURE 3 Dependence of dynein-driven corkscrewing motion on ATP concentration. (A) Microtubule rotational pitches driven by outer-arm dynein and its subparticles are plotted at various ATP concentrations. Data points and error bars are mean pitch and standard deviation respectively of the corkscrewing microtubule, driven by $\alpha\beta\gamma$ (*circle*), $\beta\gamma$ (*square*), and α (*triangle*), at 1, 3, 10, 30, and 100 μM ATP concentration. The *xyz* position of the QDs bound to microtubules was tracked every 0.05–2 s. Sliding velocity (B) and rotational velocity (C) are plotted against ATP concentration.

α-subparticles alone corkscrewed microtubules with a pitch of 1.7 μm, sliding velocity of 0.008 μm s^{-1}, and rotational velocity of 0.005 rev s^{-1}, whereas $\beta\gamma$-subparticles alone corkscrewed microtubules with a pitch of 0.8 μm (~2× shorter), sliding velocity of 0.035 μm s^{-1} (~4× faster), and rotational velocity of 0.049 rev s^{-1} (~9× faster) (Table S1). We found that corkscrewing pitch increased dramatically in a nonlinear fashion as the ratio of α-subparticle in the mixture increased (Fig. 4 *A*), and both sliding and rotational velocities decrease nonlinearly with an increasing fraction of the slower α-subparticle (Fig. 4, *B* and *C*). However, there were differences in the magnitude of the effects so that although 12.5% of slower α-subparticles in the mixture slowed the rotational velocity to 29% of the value for faster $\beta\gamma$-subparticles alone, the longitudinal velocity only slowed to 66% (Table S1). Thus, the properties of the slower α-subparticle dominate the properties of the mixture even at low molar ratios, with the effect being stronger on rotational velocity than longitudinal velocity. This is consistent with α-subparticle acting as a molecular drag on the $\beta\gamma$-subparticle and the off-axial rotational drag of the rigor state

having the strongest effect (Fig. 3). We cannot be certain that the properties of the isolated subparticles are the same as the subparticles within the three-headed $\alpha\beta\gamma$ complex. However, the properties of both the three-headed $\alpha\beta\gamma$ complex and the $\alpha+\beta\gamma$ mixture at low ATP concentrations are more like those of the α-subparticle alone, suggesting that the subparticle-like properties dominate under these conditions. Using optical trapping to quantify mechanical anisotropy in both three-headed $\alpha\beta\gamma$ and its subparticles (α and $\beta\gamma$) bound to a microtubule will provide insight into the torque-generating mechanism for these dyneins.

In contrast to previous studies, we have found that the motile properties of *Tetrahymena* outer-arm dyneins are similar to those previously reported for inner-arm dyneins (5,17). In particular, subparticles of the outer-arm dynein drive both longitudinal and rotational movement of microtubules. Observations in vivo have suggested different roles for the outer- and inner-arm dyneins in driving axonemal motion with the inner-arm dynein determining amplitude, whereas the outer-arm dyneins determine the frequency of ciliary beating (6–8). Our observations suggest that these
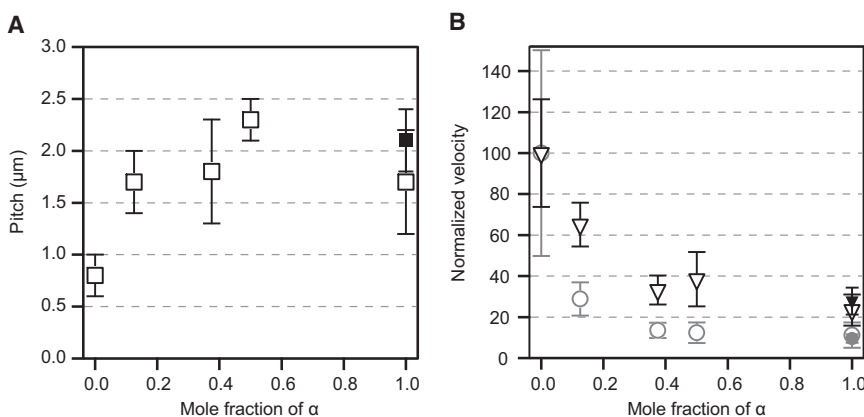

FIGURE 4 Corkscrewing motion driven by the mixture of α- and $\beta\gamma$-subparticles at 1 μM ATP. (A) Microtubule corkscrewing pitch (*open square*), (B) sliding velocity (*open triangle*), and rotational velocity (*open circle*) driven by a mixture of α and $\beta\gamma$ are plotted against the mole fraction of α. Sliding velocity and rotational velocity are normalized to 100 at mole fraction of $\alpha = 0$. Total concentration of α and $\beta\gamma$ was 0.8 μM. The solid square, triangle, and circle indicate pitch, sliding velocity, and rotational velocity driven by 1.5 μM of α alone (same condition as Fig. 3 and Table 1), respectively. Data points and error bars are mean and standard deviation.

different roles are not caused by qualitative differences in the mechanical and biochemical properties of the two sets of dyneins but rather must arise from either more subtle quantitative differences or from the different geometrical coupling of the dyneins to the microtubules within the axoneme (34,35).

SUPPORTING MATERIAL

Six figures, one table, and one movie are available at http://www.biophysj. org/biophysj/supplemental/S0006-3495(14)04816-4.

ACKNOWLEDGMENTS

REFERENCES

1. Gibbons, I. R. 1981. Cilia and flagella of eukaryotes. *J. Cell Biol.* 91:107s–124s.

2. Gibbons, I. R. 1963. Studies on the protein components of cilia from *Tetrahymena pyriformis*. *Proc. Natl. Acad. Sci. USA*. 50:1002–1010.

3. Johnson, K. A., and J. S. Wall. 1983. Structure and molecular weight of the dynein ATPase. *J. Cell Biol.* 96:669–678.

4. Kamiya, R. 2002. Functional diversity of axonemal dyneins as studied in *Chlamydomonas* mutants. *Int. Rev. Cytol.* 219:115–155.

5. Kagami, O., and R. Kamiya. 1992. Translocation and rotation of microtubules caused by multiple species of *Chlamydomonas* inner-arm dynein. *J. Cell Sci.* 103:653–664.

6. Brokaw, C. J., and R. Kamiya. 1987. Bending patterns of *Chlamydomonas* flagella: IV. Mutants with defects in inner and outer dynein arms indicate differences in dynein arm function. *Cell Motil. Cytoskeleton.* 8:68–75.

7. Mitchell, D. R., and J. L. Rosenbaum. 1985. A motile *Chlamydomonas* flagellar mutant that lacks outer dynein arms. *J. Cell Biol.* 100:1228–1234.

8. Kamiya, R., and M. Okamoto. 1985. A mutant of *Chlamydomonas reinhardtii* that lacks the flagellar outer dynein arm but can swim. *J. Cell Sci.* 74:181–191.

9. Liu, Z., H. Takazaki, …, R. Kamiya. 2008. Partially functional outer-arm dynein in a novel *Chlamydomonas* mutant expressing a truncated gamma heavy chain. *Eukaryot. Cell.* 7:1136–1145.

10. Sakakibara, H., and H. Nakayama. 1998. Translocation of microtubules caused by the alphabeta, beta and gamma outer arm dynein subparticles of *Chlamydomonas*. *J. Cell Sci.* 111:1155–1164.

11. Furuta, A., T. Yagi, …, R. Kamiya. 2009. Systematic comparison of in vitro motile properties between *Chlamydomonas* wild-type and mutant outer arm dyneins each lacking one of the three heavy chains. *J. Biol. Chem.* 284:5927–5935.

12. Sale, W. S., and L. A. Fox. 1988. Isolated beta-heavy chain subunit of dynein translocates microtubules in vitro. *J. Cell Biol.* 107:1793–1797.

13. Moss, A. G., J. L. Gatti, and G. B. Witman. 1992. The motile beta/IC1 subunit of sea urchin sperm outer arm dynein does not form a rigor bond. *J. Cell Biol.* 118:1177–1188.

14. Moss, A. G., W. S. Sale, …, G. B. Witman. 1992. The alpha subunit of sea urchin sperm outer arm dynein mediates structural and rigor binding to microtubules. *J. Cell Biol.* 118:1189–1200.

15. Vale, R. D., and Y. Y. Toyoshima. 1989. Microtubule translocation properties of intact and proteolytically digested dyneins from Tetrahymena cilia. *J. Cell Biol.* 108:2327–2334.

16. Toba, S., T. M. Gibson, …, D. J. Asai. 2004. Properties of the full-length heavy chains of *Tetrahymena* ciliary outer arm dynein separated by urea treatment. *Cell Motil. Cytoskeleton.* 58:30–38.

17. Vale, R. D., and Y. Y. Toyoshima. 1988. Rotation and translocation of microtubules in vitro induced by dyneins from *Tetrahymena* cilia. *Cell.* 52:459–469.

18. Yajima, J., K. Mizutani, and T. Nishizaka. 2008. A torque component present in mitotic kinesin Eg5 revealed by three-dimensional tracking. *Nat. Struct. Mol. Biol.* 15:1119–1121.

19. Toyoshima, Y. Y. 1987. Chymotryptic digestion of *Tetrahymena* 22S dynein. I. Decomposition of three-headed 22S dynein to one- and two-headed particles. *J. Cell Biol.* 105:887–895.

20. Toyoshima, Y. Y. 1987. Chymotryptic digestion of *Tetrahymena* ciliary dynein. II. Pathway of the degradation of 22S dynein heavy chains. *J. Cell Biol.* 105:897–901.

21. Rosenbaum, J. L., and K. Carlson. 1969. Cilia regeneration in *Tetrahymena* and its inhibition by colchicine. *J. Cell Biol.* 40:415–425.

22. Crevel, I., N. Carter, …, R. Cross. 1999. Coupled chemical and mechanical reaction steps in a processive *Neurospora* kinesin. *EMBO J.* 18:5863–5872.

23. Yajima, J., M. C. Alonso, …, Y. Y. Toyoshima. 2002. Direct long-term observation of kinesin processivity at low load. *Curr. Biol.* 12:301–306.

24. Shiroguchi, K., and Y. Y. Toyoshima. 2001. Regulation of monomeric dynein activity by ATP and ADP concentrations. *Cell Motil. Cytoskeleton.* 49:189–199.

25. Walker, R. A., E. D. Salmon, and S. A. Endow. 1990. The *Drosophila* claret segregation protein is a minus-end directed motor molecule. *Nature.* 347:780–782.

26. Yajima, J., and R. A. Cross. 2005. A torque component in the kinesin-1 power stroke. *Nat. Chem. Biol.* 1:338–341.

27. Brunnbauer, M., R. Dombi, …, Z. Ökten. 2012. Torque generation of kinesin motors is governed by the stability of the neck domain. *Mol. Cell.* 46:147–158.

28. Bormuth, V., B. Nitzsche, …, S. Diez. 2012. The highly processive kinesin-8, Kip3, switches microtubule protofilaments with a bias toward the left. *Biophys. J.* 103:L4–L6.

29. Hyman, A. A., D. Chrétien, …, R. H. Wade. 1995. Structural changes accompanying GTP hydrolysis in microtubules: information from a slowly hydrolyzable analogue guanylyl-(alpha,beta)-methylene-diphosphonate. *J. Cell Biol.* 128:117–125.

30. Meurer-Grob, P., J. Kasparian, and R. H. Wade. 2001. Microtubule structure at improved resolution. *Biochemistry.* 40:8000–8008.

31. Ray, S., E. Meyhöfer, …, J. Howard. 1993. Kinesin follows the microtubule's protofilament axis. *J. Cell Biol.* 121:1083–1093.

32. Amos, L., and A. Klug. 1974. Arrangement of subunits in flagellar microtubules. *J. Cell Sci.* 14:523–549.

33. Wilkes, D. E., H. E. Watson, …, D. J. Asai. 2008. Twenty-five dyneins in *Tetrahymena*: A re-examination of the multidynein hypothesis. *Cell Motil. Cytoskeleton.* 65:342–351.

34. Pigino, G., A. Maheshwari, …, T. Ishikawa. 2012. Comparative structural analysis of eukaryotic flagella and cilia from *Chlamydomonas*, *Tetrahymena*, and sea urchins. *J. Struct. Biol.* 178:199–206.

35. Maheshwari, A., and T. Ishikawa. 2012. Heterogeneity of dynein structure implies coordinated suppression of dynein motor activity in the axoneme. *J. Struct. Biol.* 179:235–241.

Torque generation by axonemal outer-arm dynein

Shin Yamaguchi*, Kei Saito*, Miki Sutoh*, Takayuki Nishizaka†, Yoko Y. Toyoshima* and Junichiro Yajima*‡

*Department of Life Sciences, Graduate School of Arts & Sciences, The University of Tokyo, 3-8-1 Komaba Meguro-ku,Tokyo, 153-8902, Japan; †Department of physics, Gakushuin University, 1-5-1 Mejiro, Toshima-ku, Tokyo, 171-8588, Japan.
‡Correspondence should be addressed to J.Y. (yajima@bio.c.u-tokyo.ac.jp)

Supporting figure 1; Purification of outer-arm dynein and its subparticles from *Tetrahymena* ciliary axonemes.
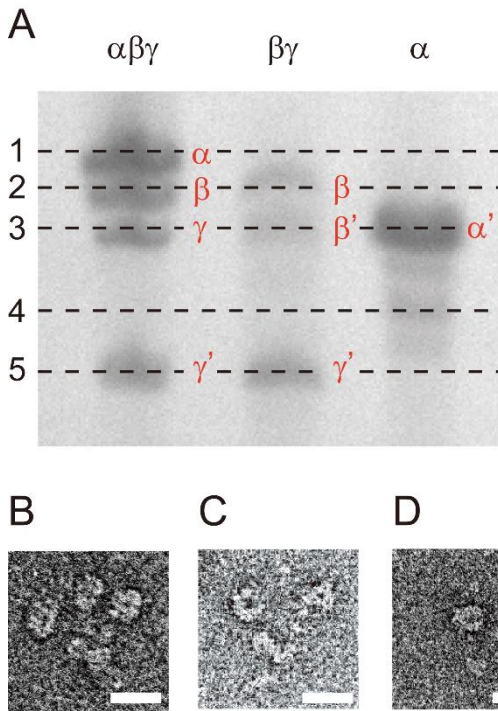
(*A*) SDS-urea-PAGE gel of purified outer-arm dynein and its subparticles. SDS-urea-PAGE was performed as described previously (1). Each dynein was loaded on a 3.2% polyacrylamide gel containing 6 M urea. Heavy chains comprising outer-arm dynein and its subparticles (α and βγ) were separated on the SDS-urea gel. Each band was numbered 1 to 5 and identified as heavy chain α, β or γ as described previously (1). α', β' and γ' mean the respective digested product of each heavy chain. (*B-D*) Negat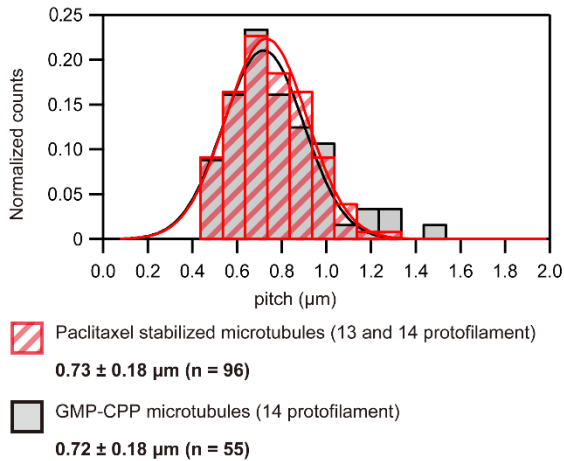ively stained EM images of purified outer-arm dynein and its subparticles. 10 µl of purified dynein (about 20 nM) was applied to carbon coated copper grids and negatively stained with 1.5% (w/v) uranyl acetate. The specimens were examined in an electron microscope (Hitachi, H-7500) at an original magnification of 40,000× operating at 80 kV. The images show purified three-headed outer-arm dynein (*B*), two-headed βγ-subparticle (*C*) and one-headed α-subparticle (*D*). However, such a bouquet structure of three-headed outer arm dynein is different from the stacked form observed in axonemes (2)(3). Scale bar, 20 nm.

**Supporting figure 2;** Tracking uncertainty of 3D measurement.
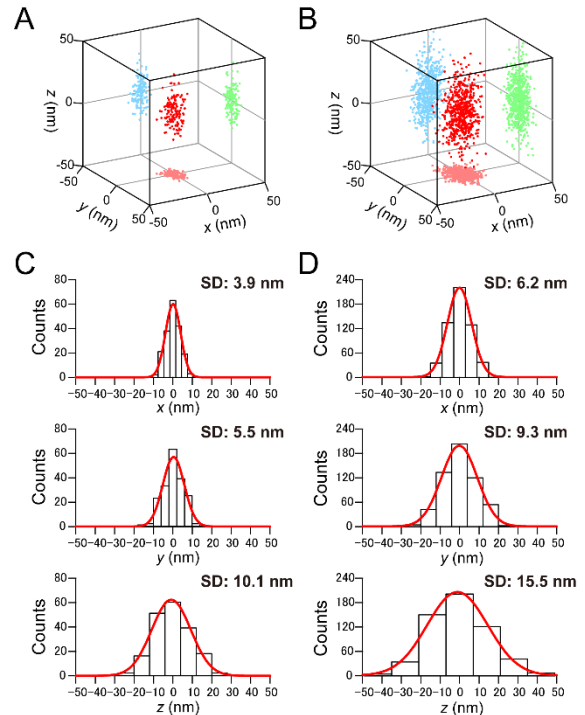
The 3D-plot shows positions of a QD attached to a microtubule fixed on a glass surface during 2 seconds at 10 frames per seconds (*A*) and 30 frames per seconds (*B*). Standard deviations (SDs) of *x*, *y* and *z* were derived from a Gaussian fitting (*C*, *D*).

Supporting figure 3; Rotational pitch of GMP-CPP microtubules.

Paclitaxel stabilized microtubules (13 and 14 protofilament)

0.73 ± 0.18 μm (n = 96)

GMP-CPP microtubules (14 protofilament)

0.72 ± 0.18 μm (n = 55)

A histogram of rotational pitch of paclitaxel stabilized microtubules (red) and GMP-CPP microtubules (black) driven by αβγ at 10 μM ATP. The pitch of GMP-CPP microtubules had a similar distribution to that of paclitaxel stabilized microtubules (p = 0.52 in *t*-test). Curves represent Gaussian fits to the data, giving mean pitches of 0.73 ± 0.18 μm (mean ± SD, paclitaxel stabilized microtubules) and 0.72 ± 0.18 μm (mean ± SD, GMP-CPP microtubules), respectively.

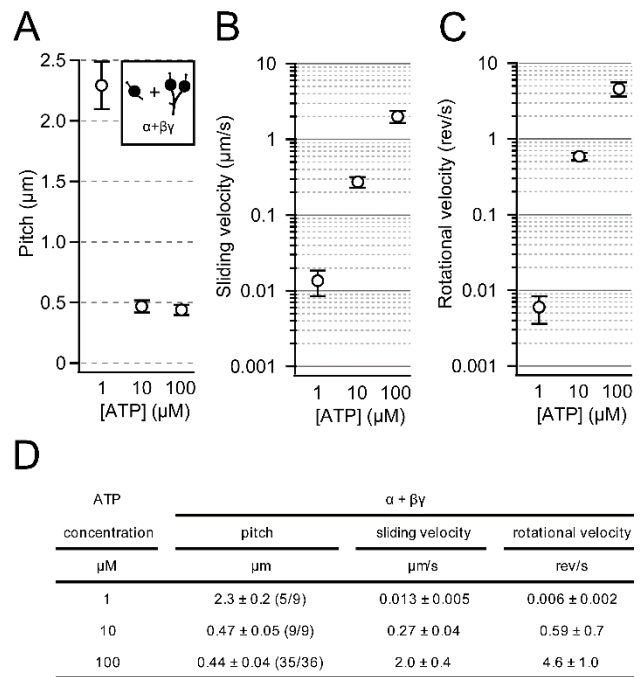**Supporting figure 4;** Relation of microtubule length to corkscrewing motion.
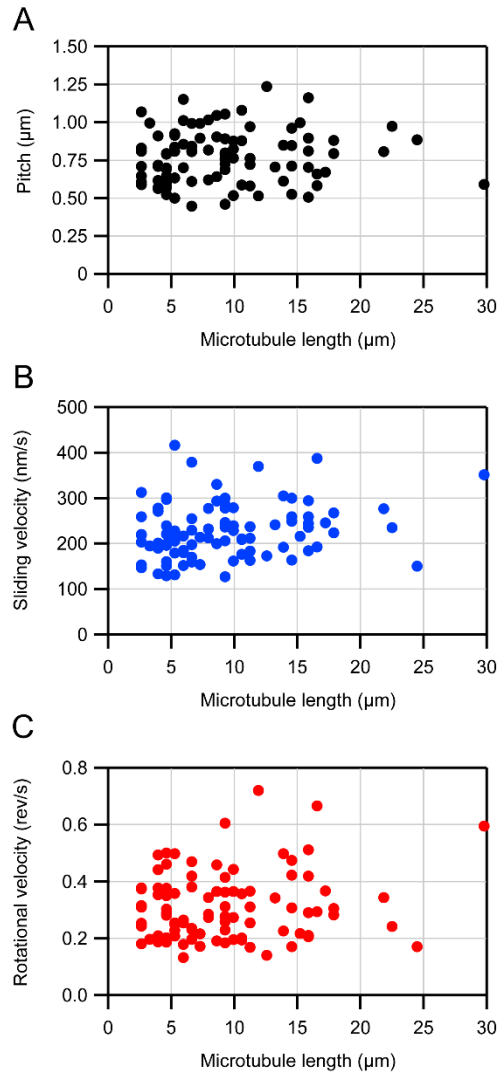
Pitch (*A*), sliding velocity (*B*) and rotational velocity (*C*) driven by αβγ at 10 μM ATP are plotted by microtubule length. Microtubule lengths were measured with the line tool of Image J (n = 90). Microtubules where the entire length was not within the field of view were rejected. Microtubule length was not correlated to the corkscrewing motion, as estimated by the Pearson correlation coefficient (R) between microtubule length and each data set. R = 0.08 (pitch), 0.22 (sliding velocity) and 0.15 (rotational velocity).

Supporting figure 5; Corkscrewing motion of a sliding microtubule driven by αβγ at 1 μM ATP and 100 μM ATP.
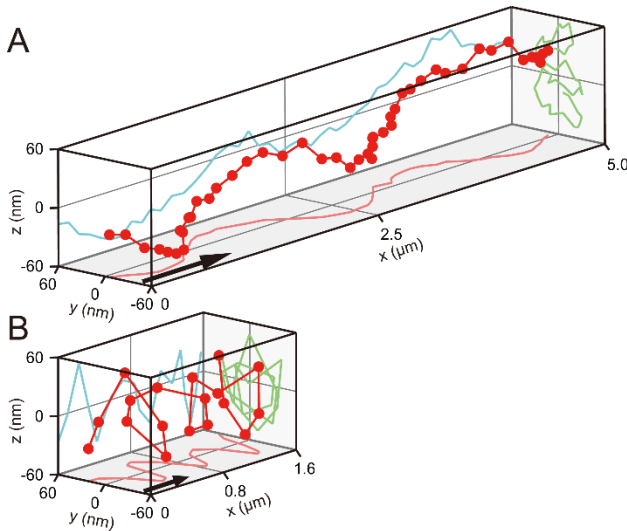
3D plot of a QD bound to a sliding microtubule driven by αβγ at 1 μM ATP (*A*) and 100 μM ATP (*B*). Images were either recorded at 2 s intervals and five images were averaged (*A*) or recorded at 0.1 s intervals with no averaging (*B*). The pitch value of corkscrewing motion is 2.0 μm (*A*) and 0.50 μm (*B*), respectively. In the presence of 1 or 100 μM ATP, αβγ is able to rotate microtubules in a clockwise manner, which is the same direction as observed in the presence of 10 μM ATP (**Fig. 1** *G*). The black arrows in (*A*) and (*B*) indicate displacement during 100 seconds (*A*) and 0.5 seconds (*B*), respectively.

Supporting figure 6; ATP concentration dependency of corkscrewing motion driven by an equimolar mixture of α and βγ.

ATP	α + βγ		
concentration	pitch	sliding velocity	rotational velocity
μM	μm	μm/s	rev/s
1	2.3 ± 0.2 (5/9)	0.013 ± 0.005	0.006 ± 0.002
10	0.47 ± 0.05 (9/9)	0.27 ± 0.04	0.59 ± 0.7
100	0.44 ± 0.04 (35/36)	2.0 ± 0.4	4.6 ± 1.0

(*A*) Microtubule rotational pitches driven by a mixture of 0.4 μM α-subparticle and 0.4 μM βγ-subparticle are plotted at 1, 10 and 100 μM ATP. Data points and error bars indicate mean pitch and standard deviation, respectively. 0.4 μM βγ and 0.4 μM α were introduced into the experimental chamber once. Sliding velocity (*B*) and rotational velocity (*C*) are plotted against ATP concentration. (*D*) Summary of corkscrewing motion driven by the mixture at 1, 10 and 100 μM ATP. Of 54 sliding QD-attached microtubules, 49 rotated. The other 5 did not rotate. Values of denominator in parentheses are the number of microtubules analyzed and values of numerator are the number of microtubules rotated. Errors are standard deviations.

Supporting table 1; Summary of corkscrewing motion driven by the mixture at 1 µM ATP.

Parameter	Value for each assay					
α (µM)	0	0.1	0.3	0.4	0.8	1.5
βγ (µM)	0.8	0.7	0.5	0.4	0	0
Mole fraction of α	0	0.125	0.375	0.5	1	1
Pitch (µm)	0.8 ± 0.2	1.7 ± 0.3	1.8 ± 0.5	2.3 ± 0.2	1.7 ± 0.5	2.1 ± 0.3
Sliding velocity (µm/s)	0.035 ± 0.009	0.023 ± 0.004	0.012 ± 0.003	0.014 ± 0.005	0.008 ± 0.003	0.010 ± 0.002
Rotational velocity (rev/s)	0.049 ± 0.024	0.014 ± 0.004	0.007 ± 0.002	0.006 ± 0.002	0.005 ± 0.003	0.005 ± 0.001
Count of microtubules analyzed	27	9	7	9	5	12
Count of microtubules corkscrewed	19	8	5	5	4	9

Supporting movie 1
The movie shows a sliding rhodamine-labeled microtubule driven by αβγ for first ~2 seconds (0.2 s intervals, actual speed, G-2A filter set, Nikon), and a moving QD fixed to the microtubule via a streptavidin-biotin interaction for remaining ~15 seconds (0.2 s intervals, ×4 actual speed, QD 525 filter set, Chroma). Image, 18 µm high, 32 µm wide.

Supporting references

1. Toyoshima, Y.Y. 1987. Chymotryptic digestion of Tetrahymena ciliary dynein. II. Pathway of the degradation of 22S dynein heavy chains. J. Cell Biol. 105: 897–901.

2. Pigino, G., A. Maheshwari, K.H. Bui, C. Shingyoji, S. Kamimura, et al. 2012. Comparative structural analysis of eukaryotic flagella and cilia from Chlamydomonas, Tetrahymena, and sea urchins. J. Struct. Biol. 178: 199–206.

3. Maheshwari, A., and T. Ishikawa. 2012. Heterogeneity of dynein structure implies coordinated suppression of dynein motor activity in the axoneme. J. Struct. Biol. 179: 235–41.